Polyoxometalate@covalent triazine framework as robust electrocatalyst for selective benzyl alcohol oxidation coupled hydrogen production

Zhen Li, Junhao Zhang, Xiaoting Jing, Jing Dong, Huifang Liu, Hongjin Lv*, Yingnan Chi*,

Changwen Hu

Contents

Fig. S1. ^{1}H NMR spectrum of monomer recorded at 298 K in DMSO.....2
Fig. S2.^{13}C CP-MAS solid state NMR spectra of CTF. 2
Fig. S3. Images of $PMo_{10}V_2$ aqueous solution (left) and **$PMo_{10}V_2$** solution after adding CTF (right).....3
Fig. S4. PXRD data of **$PMo_{10}V_2$** (red), CTF (blue), and **$PMo_{10}V_2$@CTF** (green). 3
Fig. S5. Raman spectra of CTF and **$PMo_{10}V_2$@CTF**.....3
Fig. S6. XPS spectrum of CTF. 4
Fig. S7. Survey XPS spectrum of **$PMo_{10}V_2$@CTF**.....4
Fig. S8. XPS P 2p spectra of **$PMo_{10}V_2$** and **$PMo_{10}V_2$@CTF**. 4
Fig. S9. XPS N 1s spectra of CTF. 5
Fig. S10. ^{31}P CP/MAS solid-state NMR spectra of **$PMo_{10}V_2$** and **$PMo_{10}V_2$@CTF**. 5
Fig. S11. Liquid-phase UV-vis spectra from leaching test of **$PMo_{10}V_2$@CTF** immersed in water/acetonitrile solution for 8h.....6
Fig. S12. SEM image of **$PMo_{10}V_2$@CTF**.....6
Fig. S13. N2 adsorption and desorption isotherms for CTF and **$PMo_{10}V_2$@CTF** measured at 77 K.. 6
Fig. S14. The pore size distributions (PSD) curves of CTF and **$PMo_{10}V_2$@CTF**. 7
Fig. S15. CVs of CTF without BA, or with 0.6 mmol BA. 7
Fig. S16. Gas chromatogram of benzyl alcohol oxidation. 7
Fig. S17. FT-IR spectra of **$PMo_{10}V_2$@CTF** immersed in the reaction solution for 7 days. 8
Fig. S18. UV-vis spectra of postreaction solution, benzyl alcohol, benzyl aldehyde, and **$PMo_{10}V_2$**. 8
Fig. S19. FT-IR spectra of **$PMo_{10}V_2$@CTF** before and after electrocatalytic reaction. ..8
Fig. S20. CV curves data of the Entry 2-6. 9
Fig. S21. Adsorption of benzyl alcohol by **$PMo_{10}V_2$@CTF**. 9
Fig. S22. Thermogravimetric analysis of CTF, **$PMo_{10}V_2$**, and **$PMo_{10}V_2$@CTF**. The catalyst was heated from room temperature to 800°C in N_2 atmosphere at 5°C/ min. 9
Table S1. BET surface area of different material supported polyoxometalates (POMs). 10
Table S2. Surface area and porosity data of CTF and **$PMo_{10}V_2$@CTF**. 10
Table S3. Electrocatalytic oxidation of benzyl alcohol by different electrode materials.

.....11
Table S4. Electrocatalytic oxidation of benzyl alcohol catalyzed by **$PMo_{10}V_2$@CTF** in the presence of radical scavengers. 11
Reference.....12

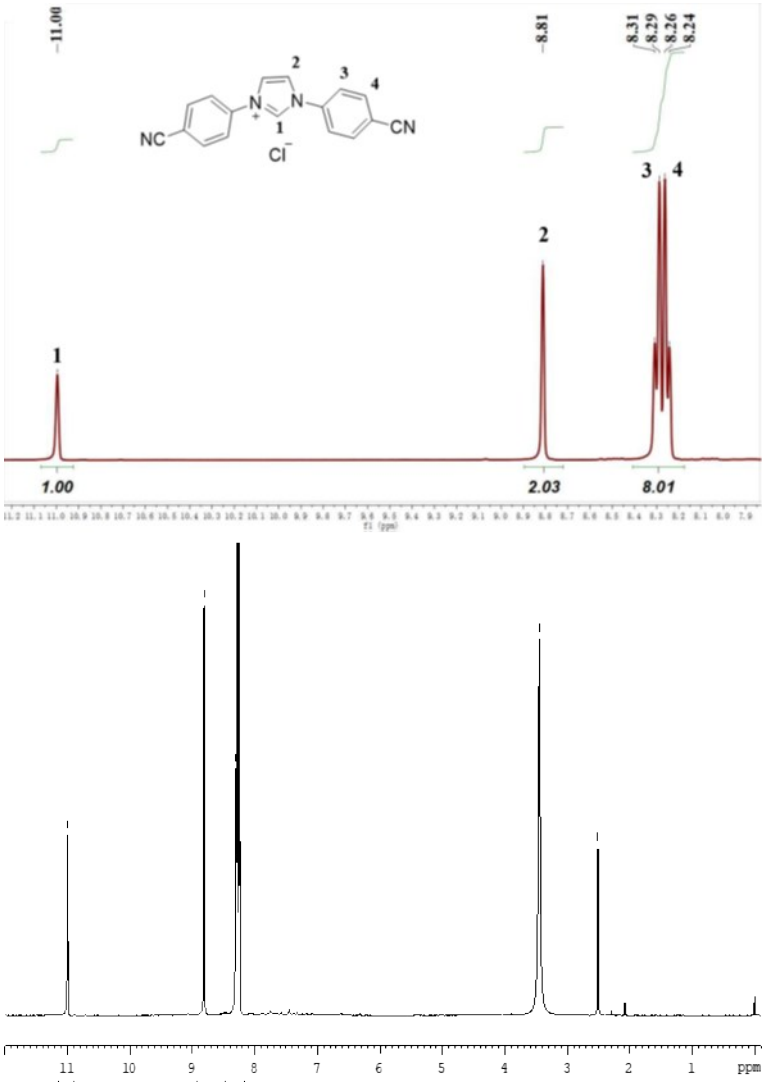

Fig. S1. ^{1}H NMR spectrum of monomer recorded at 298 K in DMSO.

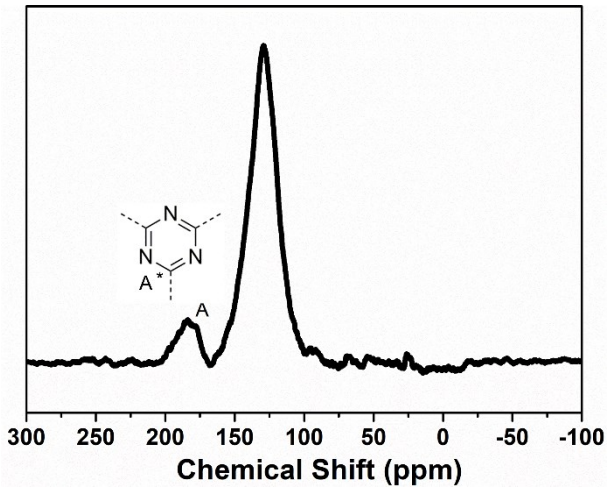

Fig. S2.^{13}C CP-MAS solid state NMR spectra of CTF.

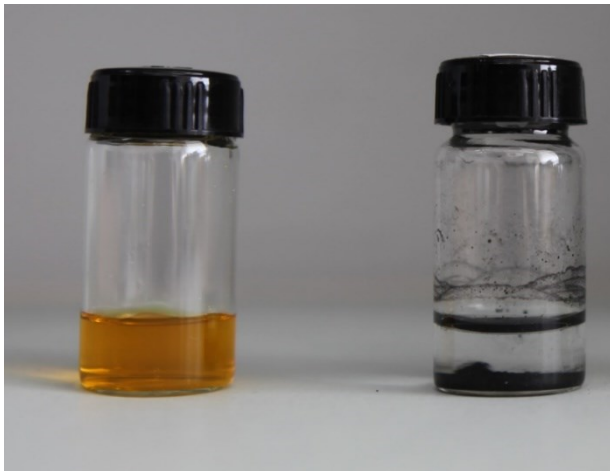

Fig. S3. Images of **$PMo_{10}V_2$** aqueous solution (left) and **$PMo_{10}V_2$** solution after adding CTF (right).

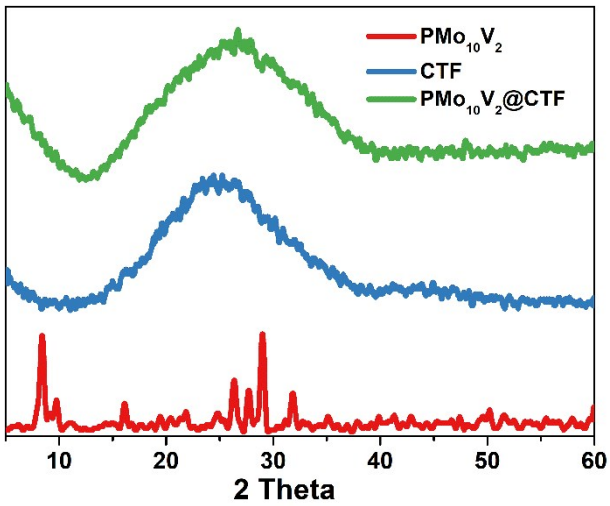

Fig. S4. PXRD data of **$PMo_{10}V_2$** (red), CTF (blue), and **$PMo_{10}V_2$@CTF** (green).

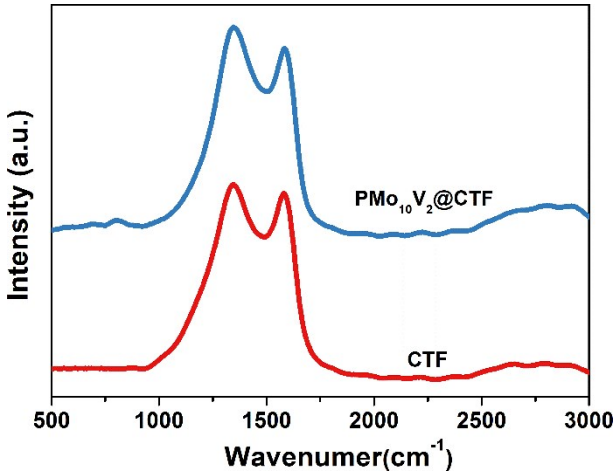

Fig. S5. Raman spectra of CTF and **$PMo_{10}V_2$@CTF**.

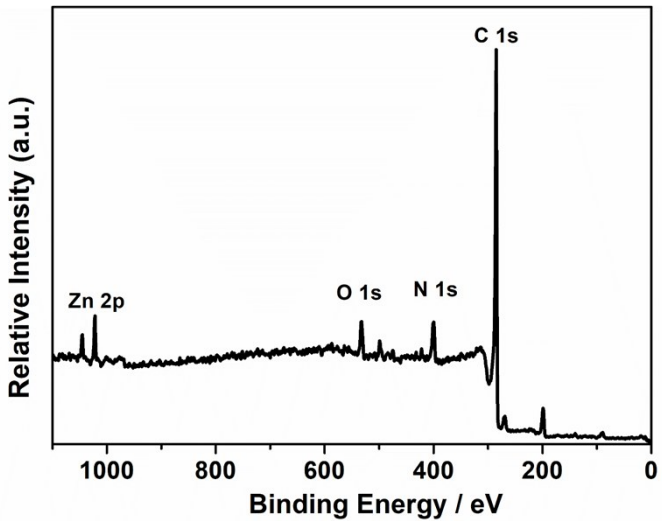

Fig. S6. XPS spectrum of CTF.

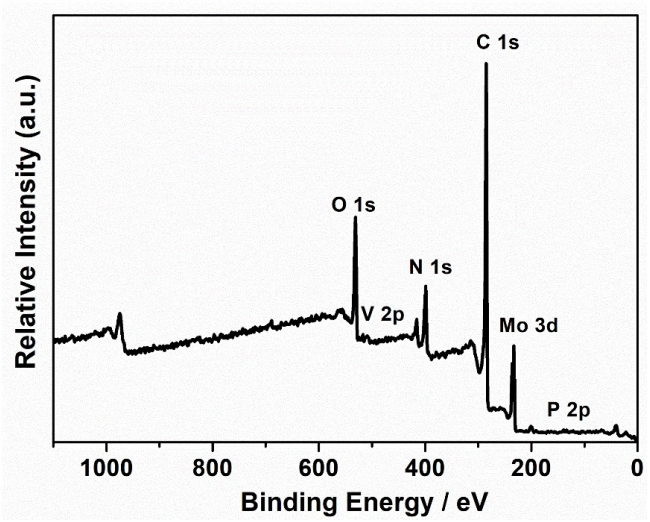

Fig. S7. Survey XPS spectrum of **$PMo_{10}V_2$@CTF**.

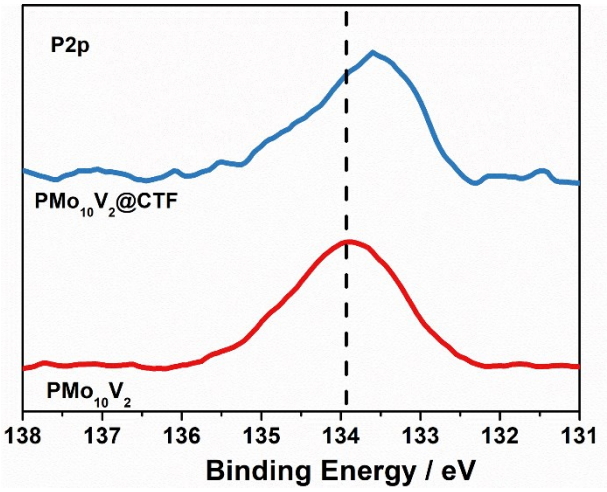

Fig. S8. XPS P 2p spectra of **$PMo_{10}V_2$** and **$PMo_{10}V_2$@CTF**.

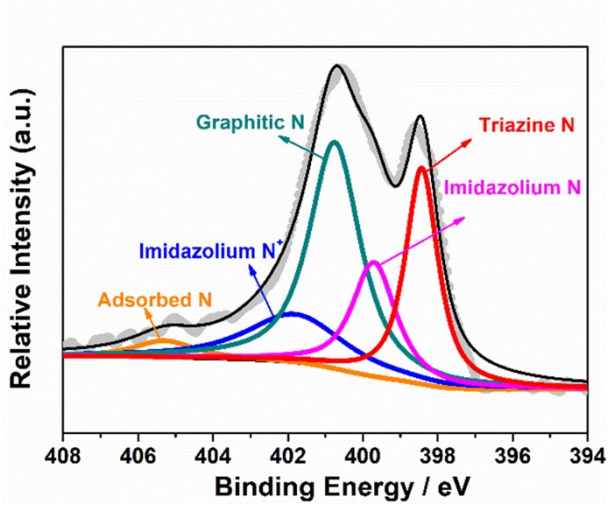

Fig. S9. XPS N 1s spectra of CTF. The XPS N 1s spectrum of CTF can be deconvoluted into five peaks at 398.4 eV, 399.7 eV, 400.7 eV, 401.9 eV and 405.4 eV which are assigned to triazinic N, imidazolium N, graphitic N, imidazolium N^+ and absorbed N, respectively.

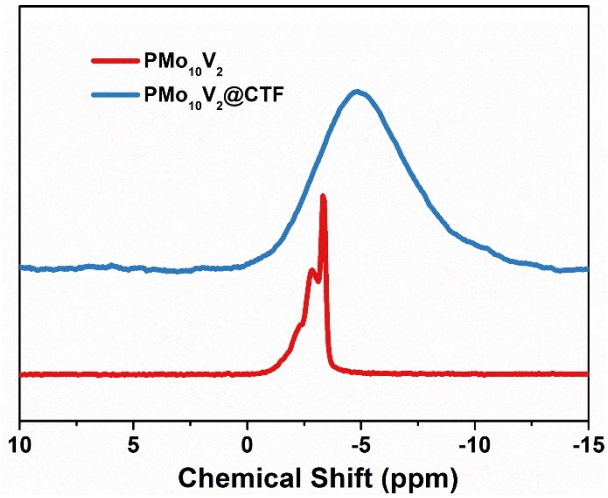

Fig. S10. ^{31}P CP/MAS solid-state NMR spectra of **$PMo_{10}V_2$** and **$PMo_{10}V_2$@CTF**.

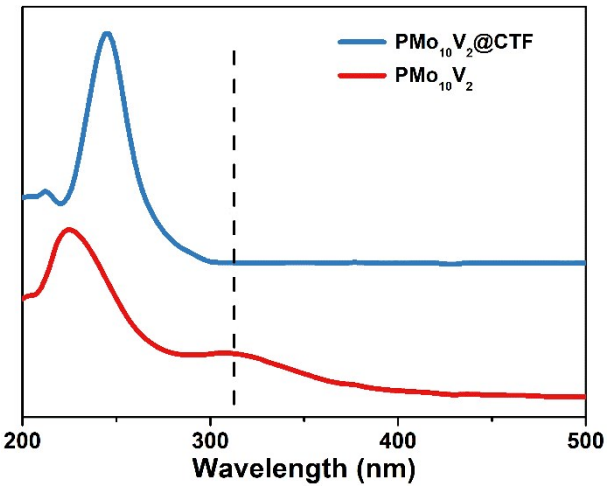

Fig. S11. Liquid-phase UV-vis spectra from leaching test of **$PMo_{10}V_2$@CTF** immersed in water/acetonitrile solution for 8h.

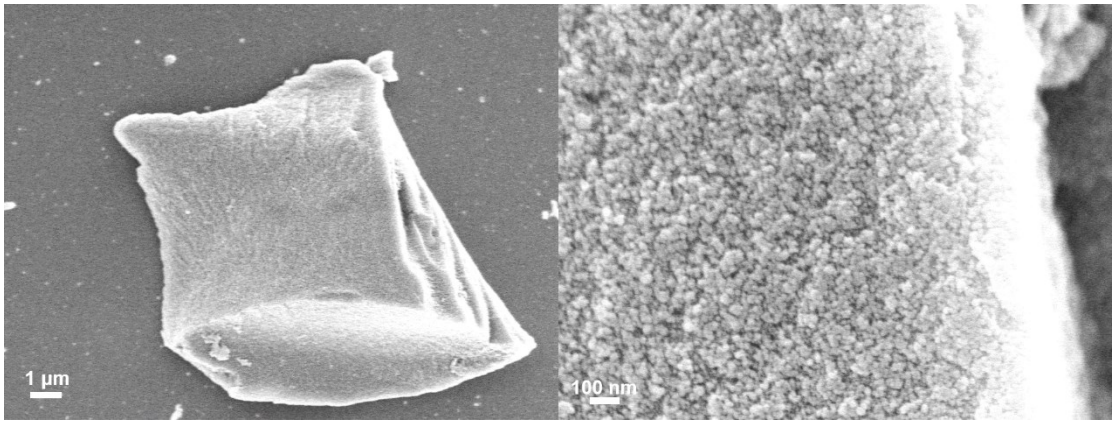

Fig. S12. SEM image of **$PMo_{10}V_2$@CTF**.

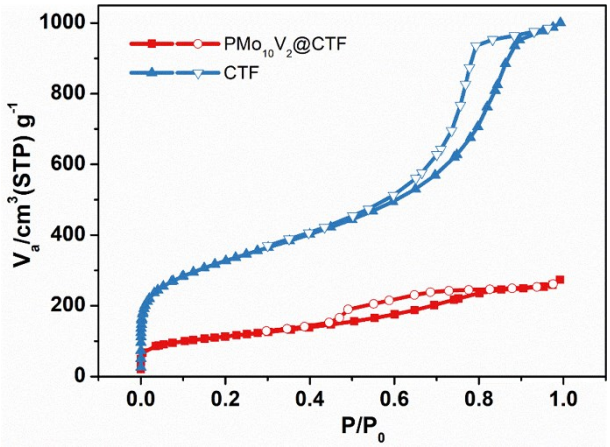

Fig. S13. N2 adsorption and desorption isotherms for CTF and **$PMo_{10}V_2$@CTF** measured at 77 K.

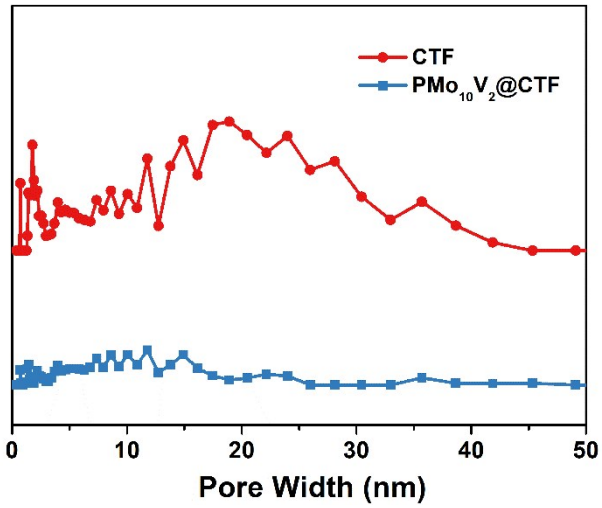

Fig. S14. The pore size distributions (PSD) curves of CTF and **$PMo_{10}V_2$@CTF**.

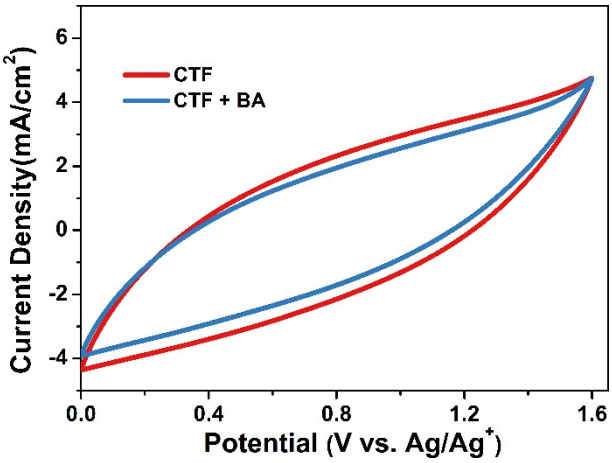

Fig S15. CV curves of CTF in acetonitrile containing $LiClO_4$ (1.5 mmol) without benzyl alcohol (BA) and with 0.6 mmol BA, obtained at carbon cloth working electrode with a scan rate of 50 mV s^{-1}.

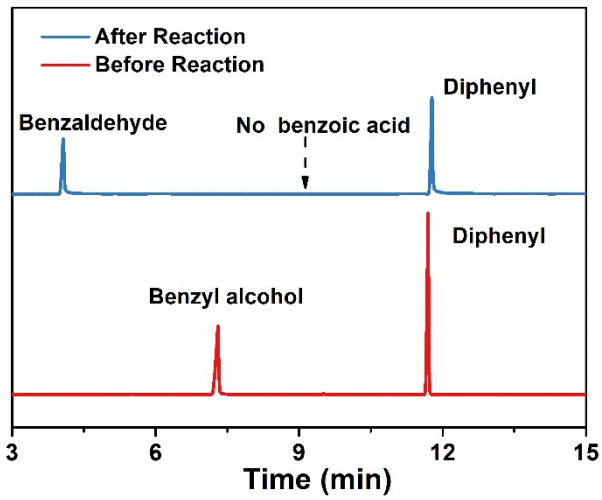

Fig. S16. Gas chromatogram of benzyl alcohol oxidation.

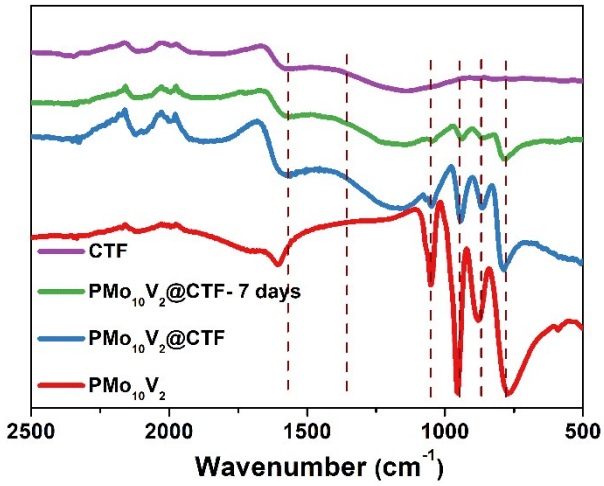

Fig. S17. FT-IR spectra of **$PMo_{10}V_2$@CTF** immersed in the reaction solution for 7 days.

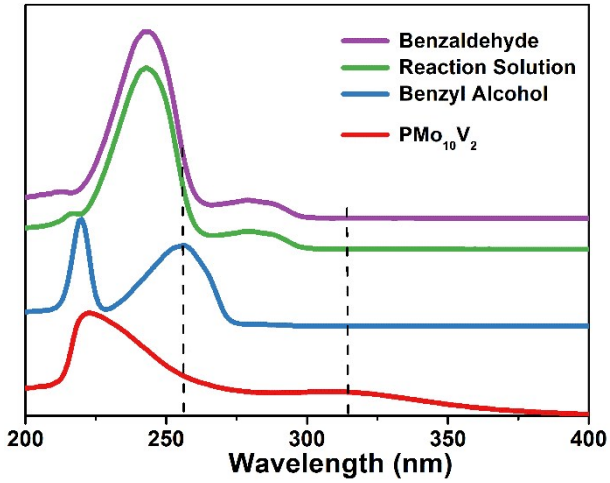

Fig. S18. UV-vis spectra of postreaction solution, benzyl alcohol, benzyl aldehyde, and **$PMo_{10}V_2$**.

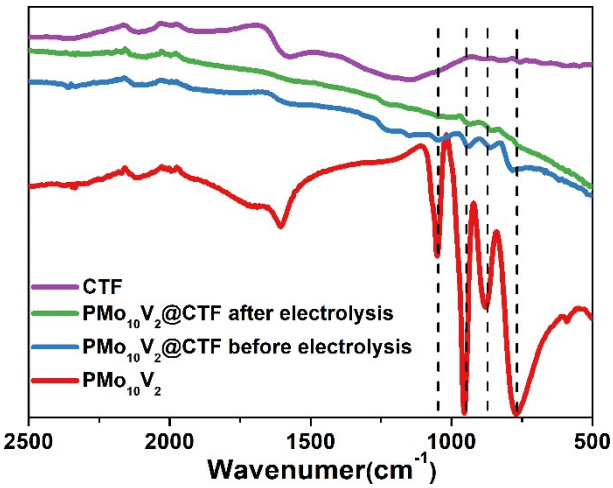

Fig. S19. FT-IR spectra of **$PMo_{10}V_2$@CTF** before and after electrocatalytic reaction.

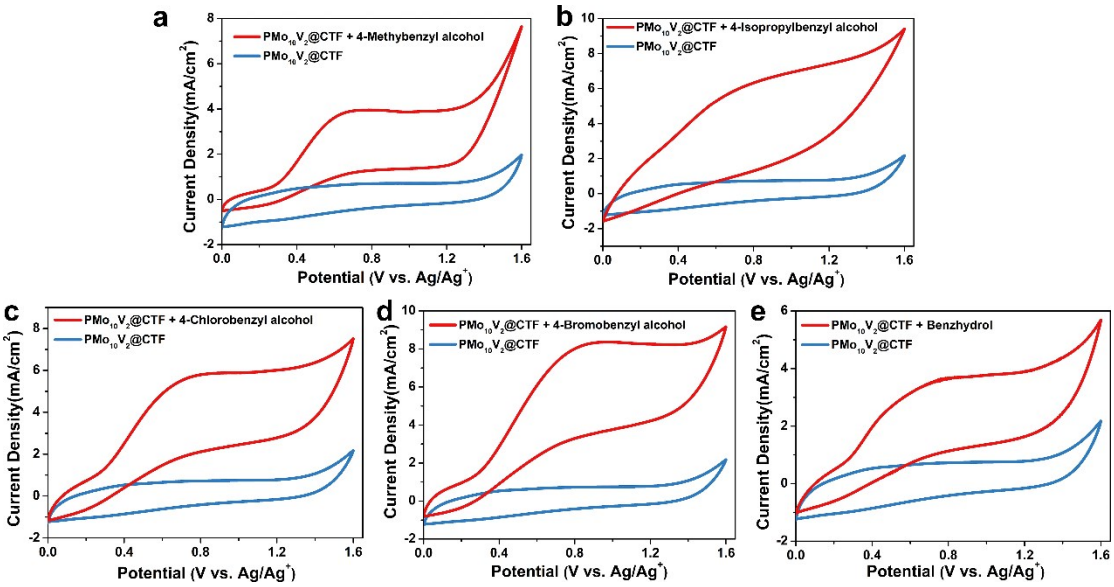

Fig. S20. CV curves of **$PMo_{10}V_2$@CTF** without benzylic alcohols (blue lines) and with 0.6 mmol benzylic alcohols (red lines) in acetonitrile containing $LiClO_4$ (1.5 mmol) and Et_3N (0.18 mmol) obtained at carbon cloth working electrode modified with **$PMo_{10}V_2$@CTF** (0.3 mg/cm^2) with a scan rate of 50 mV s^{-1}.

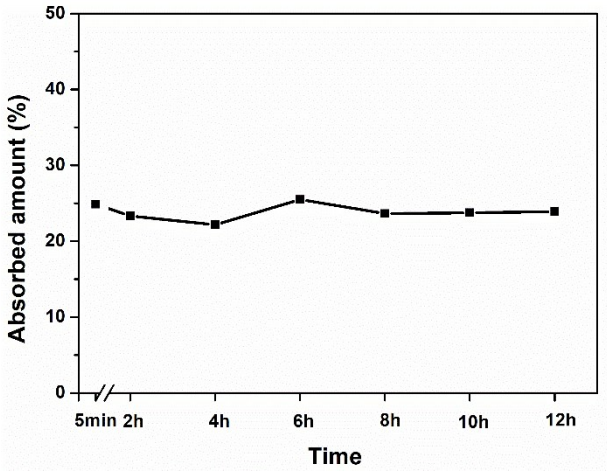

Fig. S21. Adsorption of benzyl alcohol by **$PMo_{10}V_2$@CTF**.

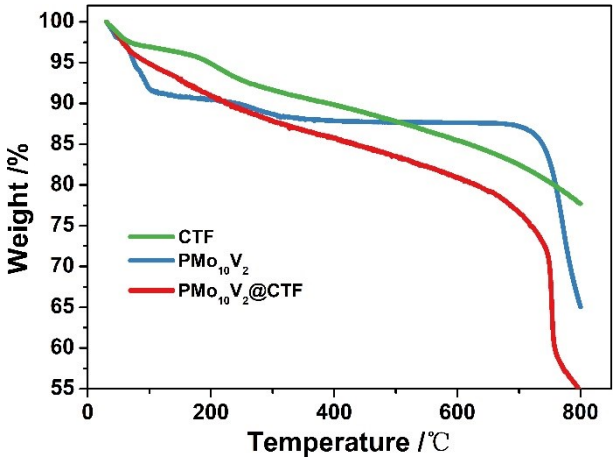

Fig. S22. Thermogravimetric analysis of CTF, **$PMo_{10}V_2$**, and **$PMo_{10}V_2$@CTF**.

Table S1. BET surface area of different material supported polyoxometalates (POMs).

Entry	Material	Surface area ($m^2\ g^{-1}$)	Reference
1	$PMo_{10}V_2$@CTF	399	This work
2	POM@ZIF-8 [a]	411	1
3	CsPW-HMS [b]	117	2
4	NENU-500 [c]	195	3
5	Mg_3Al-ILs-C_8-LaW_{10} [d]	63	4
6	PMo/BzPN-SiO_2 [e]	122	5
7	SiO_2@C-dots/QPW5501	110	6
8	V_8@iPAF-1 [g]	670	7
9	EB-COF:PW_{12} [h]	8	8

[a] POM : $H_6CoW_{12}O_{40}$

[b] CsPW: $Cs_{2.5}H_{0.5}PW_{12}O_{40}$

[c] NENU-500: $[TBA]_3[\varepsilon\text{-}PMo^{V}_{8}Mo^{VI}_{4}O_{36}(OH)_4Zn_4][BTB]_{4/3}\cdot x$Guest (BTB = benzene tribenzoate, TBA^+ = tetrabutylammonium ion)

[d] LaW_{10}: $Na_9LaW_{10}O_{36}\cdot 32\ H_2O$

[e] PMo: $H_3PMo_{12}O_{40}$

[f] PW5501: Commercial $H_3PW_{12}O_{40}$ (2 g) was calcined at 550 °C for 1 h

[g] V_8: $(NH_4)_5H_6PV_8Mo_4O_{40}$

[h] PW_{12}: $H_3PW_{12}O_{40}$

Table S2. Surface area and porosity data of CTF and **$PMo_{10}V_2$@CTF**.

Entry	Material	Surface area ($m^2\ g^{-1}$)	Pore size (nm)	Pore volume ($cm\ g^{-1}$)
1	CTF	1154	5.353	1.813
2	$PMo_{10}V_2$@CTF	399	4.222	0.582

Table S3. Electrocatalytic oxidation of benzyl alcohol by different electrode materials.

Entry	Catalysts	Co-catalyst	Conv.	Sele.	Time	FE.	Ref.
1	$PMo_{10}V_2$@CTF	none	>99	>99	12 h	96 %	This work
2	h-$Ni(OH)_2$	TEMPO	90	94	40 min	76%	[9]
3	NC@$CuCo_2N_x$/CF[a]	TEMPO	97	95	80 min	81%	[10]
4	HP-2[b]	TEMPO	–	–	–	97 %	[11]
5	CNT/MOL[c]	TEMPO	100	100	100 min	–	[12]
6	TEMPO-MCM-41[d]	none	100	100	100 min	–	[13]

"– ": there is no corresponding data in the report.

TEMPO: 2,2,6,6-tetramethylpiperidine-N-oxyl

[a] NC@$CuCo_2N_x$/CF: nitrogen-doped carbon (NC)@$CuCo_2N_x$/carbon fiber (CF)

[b] HP-2: poly(2,2,6,6-tetramethylpiperidinyloxy-4-yl methacrylate) (HP-2)

[c] CNT/MOL: fabricated by Hf-MOF layers and multiwalled carbon nanotubes.

[d] TEMPO-MCM-41: TEMPO-functionalized ordered mesoporous silica (MCM-41)

The conversion of benzyl alcohol, selectivity to aldehyde, Faraday efficiency, reaction time from recent investigations using different electrode materials have been summarized in Table S3. It is found that the good performance of most reported electrocatalytic materials was achieved in the presence of stoichiometric TEMPO, a homogeneous co-catalyst, (entries 2-5). In comparison, there is no TEMPO added in our reaction system and the conversion, selectivity, and Faraday efficiency are comparable to and even better than the reported data. However, the reaction time of our system is longer than previous reports.

Table S4. Electrocatalytic oxidation of benzyl alcohol catalyzed by **$PMo_{10}V_2$@CTF** in the presence of radical scavengers[a].

Entry	Scavenger	Conversion (%)	Selectivity (%)
1	Ph_2NH (0.6 mmol)	35	3
2	tert-butyl alcohol (0.6 mmol)	90	80

[a]Reaction conditions: BA (0.6 mmol), anhydrous acetonitrile (10 mL), Et_3N (0.18 mmol), and $LiClO_4$ (1.5 mmol) at ambient conditions for 12 h with the potential of 1.6 V vs. Ag/Ag^+

Reference

1. S. Mukhopadhyay, J. Debgupta, C. Singh, A. Kar and S. K. Das, *Angew Chem Int Ed Engl*, 2018, **57**, 1918-1923.
2. T. Okada, K. Miyamoto, T. Sakai and S. Mishima, *ACS Catalysis*, 2013, **4**, 73-78.
3. J. S. Qin, D. Y. Du, W. Guan, X. J. Bo, Y. F. Li, L. P. Guo, Z. M. Su, Y. Y. Wang, Y. Q. Lan and H. C. Zhou, *J. Am. Chem. Soc.*, 2015, **137**, 7169-7177.
4. Z. W. Tengfei Li, Wei Chen, Haralampos N. Miras, and Yu-Fei Song, *Chemistry A European Journal*, 2017, **23**, 1069-1077.
5. M. Craven, D. Xiao, C. Kunstmann-Olsen, E. F. Kozhevnikova, F. Blanc, A. Steiner and I. V. Kozhevnikov, *Applied Catalysis B: Environmental*, 2018, **231**, 82-91.
6. Y. Zhang and R. Wang, *Applied Catalysis B: Environmental*, 2018, **234**, 247-259.
7. J. Song, Y. Li, P. Cao, X. Jing, M. Faheem, Y. Matsuo, Y. Zhu, Y. Tian, X. Wang and G. Zhu, *Adv. Mater.*, 2019, **31**, e1902444.
8. H. Ma, B. Liu, B. Li, L. Zhang, Y. G. Li, H. Q. Tan, H. Y. Zang and G. Zhu, *J. Am. Chem. Soc.*, 2016, **138**, 5897-5903.
9. X. Chen, X. Zhong, B. Yuan, S. Li, Y. Gu, Q. Zhang, G. Zhuang, X. Li, S. Deng and J.-g. Wang, *Green Chemistry*, 2019, **21**, 578-588.
10. J. Zheng, X. Chen, X. Zhong, S. Li, T. Liu, G. Zhuang, X. Li, S. Deng, D. Mei and J.-G. Wang, *Adv. Funct. Mater.*, 2017, **27**, 1704169.
11. B. Schille, N. O. Giltzau and R. Francke, *Angew Chem Int Ed Engl*, 2018, **57**, 422-426.
12. L. Yang, L. Cao, R. Huang, Z. W. Hou, X. Y. Qian, B. An, H. C. Xu, W. Lin and C. Wang, *ACS Appl Mater Interfaces*, 2018, **10**, 36290-36296.
13. B. Karimi, M. Rafiee, S. Alizadeh and H. Vali, *Green Chemistry*, 2015, **17**, 991-1000.